Consequences of nanofluid on Peristaltic flow in an asymmetric channel

Safia Akram[1], *S. Nadeem* [2] , *Abdul Ghafoor* [3] *Changhoon Lee* [4]

[1] *Department of Basic Sciences, MCS, National University of Sciences and Technology, Rawalpindi* 46000 *, Pakistan*

[2] *Department of Mathematics, Quaid-i-Azam University* 45320 *, Islamabad* 44000 *Pakistan*

[3] *Department of Electrical Engineering, MCS, National University of Sciences and Technology, Rawalpindi* 46000 *, Pakistan*

[4] *Department of Computational Sciences and Engineering, Yonsei University Seoul, Korea*

Abstract: In the present analysis we have discussed the peristaltic flow of a nanofluid in an asymmetric channel. The governing equations of a nanofluid are first modeled and then simplified under the assumption of long wave length and low Reynolds number approximation. The governing equations of temperature and nano particle volume fraction are coupled and solved analytically using a Homotopy perturbation method. The exact solution have been calculated for the stream functions,, velocity profile and pressure gradient. In the end graphical results are discussed for five different wave forms to see the effects of various physical parameters of interest.

Keywords: Peristaltic flow, nanofluid particles, Jeffrey fluid model, different wave forms, asymmetric channel.

Introduction

The peristaltic transport (traveling contraction wave along a tube-like structure) results physiologically from neuromuscular properties of tubular smooth muscle. It is well known major mechanisms for fluid transport in many biological systems like swallowing food through the esophagus, urine transport from the kidney to the bladder through the ureter, movement of chyme in the gastrointestinal tract, movement of ovum in the female fallopian tubes, the transport of spermatozoa in the ducts efferentes of the male reproductive tracts and in the cervical canal, the transport of lymph in the lymphatic vessels, and the vasomotion in small blood vessels such as arterioles, venues and capillaries [1] . It also occurs in many applications involving biomedical systems and behaves in general like suspensions (for example, blood is a suspension of red cells, white cells, and platelets in plasma, cervical mucus is a suspension of macromolecules in a water-like liquid [2]) of deformable or rigid particles in a fluid. The biviscosity fluid can represent the behavior of blood in vessels of small diameter as the mean shear rate is about 20--150 $s-1$ [3] . The researchers have examined both theoretical and experimental aspects of the peristaltic flows keeping different flow geometries and different fluids. Mention may be made to the interesting works of [4−17].

The study of nanofluids is another important area which has attracted the attention of researchers. Nanofluidics is often defined as the study and application of fluid flow in and around nano-sized objects. Its environments/applications include biological organisms on their primary cellular level, snapping shrimps and super-hydrophobic beetle wings, use of charged

[1]Corresponding author: E-mail: safia_akram@yahoomail.com (Safia Akram)

polymers for lubrication, the lotus effect for self-cleaning surfaces, membranes for filtering on size or charge (e.g. for desalination) and nanoporous materials for size exclusion chromatography, passive selective transport in aquaporins and active transport in ion channels, molecular motors like kinesis and charge based filtration in the kidney basal membrane, etc [18] . Since the first investigation done by Choi [19] in this discipline, number of researchers have focused their attention to this area. Recently, Makinde and Aziz [20] have examined the boundary layer flow of a nanofluid past a stretching sheet with a convective boundary condition. Boundary layer flow of nanofluid over a moving surface in a flowing fluid has been investigated by Bachok et el [21] . Some other is cited in the Ref. [22 – 25].

Motivated from the above studies, we have discussed the peristaltic flow of non-Newtonian nanofluid in an asymmetric channel. The governing flow equations are modelled and simplified under the assumption of long wave length and low Reynolds number approximation. The equations of temperature and nano-particle volume fraction are coupled and solved analytically using a Homotopy perturbation method. The exact solutions have been calculated for the stream functions, velocity profile and pressure gradient. In the end graphical results are discussed for five different wave forms (Sinusoidal, Multisinusoidal, Triangular, Trapezoidal, and Square wave) to see the effects of various physical parameters of interest.

Mathematical Formulation

Let us consider the peristaltic transport of an incompressible Jeffrey fluid in a two dimensional channel of width $d_1 + d_2$. Since we are considering asymmetric channel therefore, the channel flow is produced due to different amplitudes and phases of the peristaltic waves on the channel. Heat transfer along with nano particle phenomena has been taken into account. The lower wall of the channel is maintained at temperature T_1 and nano particle volume fraction C_1 while the upper wall has temperature T_0 and nano particle volume fraction C_0.

The geometry of the wall surface is defined as

$$Y = H_1 = d_1 + a_1 \cos\left[\frac{2\pi}{\lambda}(X - ct)\right], Y = H_2 = -d_2 - b_1 \cos\left[\frac{2\pi}{\lambda}(X - ct) + \phi\right], \quad (1)$$

where a_1 and b_1 are the amplitudes of the waves, λ is the wave length, $d_1 + d_2$ is the width of the channel, c is the velocity of propagation, t is the time and X is the direction of wave propagation, the phase difference ϕ varies in the range $0 \le \phi \le \pi, \phi = 0$ corresponds to symmetric channel with waves out of phase and $\phi = \pi$ the waves are in phase, and further a_1, b_1, d_1, d_2 and ϕ satisfies the condition

$$a_1^2 + b_1^2 + 2a_1 b_1 \cos\phi \le (d_1 + d_2)^2.$$

The equations governing the flow for an incompressible nanofluid are given by [20]

$$\frac{\partial U}{\partial X}+\frac{\partial V}{\partial Y}=0, \tag{2}$$

$$\rho\left(\frac{\partial U}{\partial t}+U\frac{\partial U}{\partial X}+V\frac{\partial U}{\partial Y}\right)=-\frac{\partial P}{\partial X}+\frac{\partial}{\partial X}\left(S_{XX}\right)+\frac{\partial}{\partial Y}\left(S_{XY}\right)+\rho g\alpha\left(T_1-T_0\right)+\rho g\alpha\left(C_1-C_0\right), \tag{3}$$

$$\rho\left(\frac{\partial V}{\partial t}+U\frac{\partial V}{\partial X}+V\frac{\partial V}{\partial Y}\right)=-\frac{\partial P}{\partial Y}+\frac{\partial}{\partial X}\left(S_{YX}\right)+\frac{\partial}{\partial Y}\left(S_{YY}\right), \tag{4}$$

$$c_p\left(\frac{\partial T}{\partial t}+U\frac{\partial T}{\partial X}+V\frac{\partial T}{\partial Y}\right)=\frac{K'}{\rho}\left(\frac{\partial^2 T}{\partial X^2}+\frac{\partial^2 T}{\partial Y^2}\right)+\tau\left\{D_B\left(\frac{\partial C}{\partial X}\frac{\partial T}{\partial X}+\frac{\partial C}{\partial Y}\frac{\partial T}{\partial Y}\right)\left(\frac{D_T}{T_0}\right)\left[\left(\frac{\partial T}{\partial X}\right)^2+\left(\frac{\partial T}{\partial Y}\right)^2\right]\right\}, \tag{5}$$

$$\left(\frac{\partial C}{\partial t}+U\frac{\partial C}{\partial X}+V\frac{\partial C}{\partial Y}\right)=D_B\left(\frac{\partial^2 C}{\partial X^2}+\frac{\partial^2 C}{\partial Y^2}\right)+\left(\frac{D_T}{T_0}\right)\left(\frac{\partial^2 T}{\partial X^2}+\frac{\partial^2 T}{\partial Y^2}\right) \tag{6}$$

where U , V are the velocities in X and Y directions in fixed frame, ρ is constant density, P is the pressure, ν is the kinematic viscosity, K' is the thermal conductivity, c_p is the specific heat, T is the temperature, D_B is the Brownian diffusion coefficient, D_T is the thermophoretic diffusion coefficient and $\tau=\frac{(\rho c)_p}{(\rho c)_f}$ is the ratio of the effective heat capacity of the nanoparticle material and heat capacity of the fluid with ρ being the density, c is the volumetric volume expansion coefficient and ρ_p is the density of the particles.

The constitutive equation for the extra stress tensor $\mathbf{S}$ is

$$\mathbf{S}=\frac{\mu}{1+\lambda_1}\left(\dot{\gamma}+\lambda_2\ddot{\gamma}\right). \tag{7}$$

In above equation λ_1 is the ratio of relaxation to retardation times, $\dot{\gamma}$ the shear rate, λ_2 the retardation time and dots denote the differentiation with respect to time.

Introducing a wave frame (x,y) moving with velocity c away from the fixed frame (X,Y) by the transformation

$$x=X-ct,\ y=Y,\ u=U-c,\ v=V,\ \text{and}\ p(x)=P(X,t). \tag{8}$$

Defining

$$\bar{x}=\frac{x}{\lambda},\ \bar{y}=\frac{y}{d_1},\ \bar{u}=\frac{u}{c},\ \bar{v}=\frac{v}{c},\ \delta=\frac{d_1}{\lambda},\ d=\frac{d_2}{d_1},\ \bar{p}=\frac{d_1^2 p}{\mu c\lambda},\ \bar{t}=\frac{ct}{\lambda},\ h_1=\frac{H_1}{d_1},$$

$$h_2=\frac{H_2}{d_2},\ a=\frac{a_1}{d_1},\ b=\frac{b_1}{d_1},\ R_e=\frac{cd_1}{\nu},\ \overline{\Psi}=\frac{\Psi}{cd_1},\ \theta=\frac{T-T_0}{T_1-T_0},\ \bar{S}=\frac{Sd_1}{\mu c},$$

$$\alpha=\frac{K'}{c_p\rho},\ \Pr=\frac{\nu}{\alpha},\ N_T=\frac{\tau D_T\left(T_1-T_0\right)}{T_0\nu},\ N_b=\frac{\tau D_B\left(C_1-C_0\right)}{\upsilon},$$

$$Gr=\frac{\rho g\alpha d_1^2\left(T_1-T_0\right)}{\mu c},\ B_r=\frac{\rho g\alpha d_1^2\left(C_1-C_0\right)}{\mu c}. \tag{9}$$

Using the above non-dimensional quantities the resulting equations in terms of stream function Ψ(dropping the bars, $u = \frac{\partial \Psi}{\partial y}, v = -\delta \frac{\partial \Psi}{\partial x}$) can be written as

$$\mathrm{Re}\,\delta\left(\Psi_y\Psi_{xy} - \Psi_x\Psi_{yy}\right) = -\frac{\partial p}{\partial x} + \delta\frac{\partial}{\partial x}\left(S_{xx}\right) + \frac{\partial}{\partial y}\left(S_{xy}\right) + Gr\theta + B_r\Phi, \tag{10}$$

$$\mathrm{Re}\,\delta^3\left(-\Psi_y\Psi_{xx} + \Psi_x\Psi_{xy}\right) = -\frac{\partial p}{\partial y} + \delta^2\frac{\partial}{\partial x}\left(S_{yx}\right) + \delta\frac{\partial}{\partial y}\left(S_{yy}\right), \tag{11}$$

$$\begin{aligned}\mathrm{Re}\,\delta\left(\Psi_y\theta_x - \Psi_x\theta_y\right) &= \frac{1}{\mathrm{Pr}}\left(\theta_{yy} + \delta^2\theta_{xx}\right) + N_b\left(\delta^2\theta_x\Phi_x + \theta_y\Phi_y\right)\\ &\quad + N_T\left(\delta^2\left(\theta_x\right)^2 + \left(\theta_y\right)^2\right),\end{aligned} \tag{12}$$

$$\mathrm{Re}\,\delta\left(\Psi_y\theta_x - \Psi_x\theta_y\right) = \left(\Phi_{yy} + \delta^2\Phi_{xx}\right) + \delta^2\frac{N_T}{N_b}\theta_{xx} + \frac{N_T}{N_b}\theta_{yy}, \tag{13}$$

where

$$\begin{aligned}S_{xx} &= \frac{2\delta}{1+\lambda_1}\left(1 + \frac{\lambda_2 c\delta}{d_1}\left(\Psi_y\frac{\partial}{\partial x} - \Psi_x\frac{\partial}{\partial y}\right)\right)\Psi_{xy},\\ S_{xy} &= \frac{1}{1+\lambda_1}\left(1 + \frac{\lambda_2 c\delta}{d_1}\left(\Psi_y\frac{\partial}{\partial x} - \Psi_x\frac{\partial}{\partial y}\right)\right)\left(\Psi_{yy} - \delta^2\Psi_{xx}\right),\\ S_{yy} &= -\frac{2\delta}{1+\lambda_1}\left(1 + \frac{\lambda_2 c\delta}{d_1}\left(\Psi_y\frac{\partial}{\partial x} - \Psi_x\frac{\partial}{\partial y}\right)\right)\Psi_{xy}.\end{aligned} \tag{14}$$

The corresponding boundary conditions are

$$\begin{aligned}\Psi &= \frac{q}{2} \text{ at } y = h_1 = 1 + a\cos 2\pi x,\\ \Psi &= -\frac{q}{2} \text{ at } y = h_2 = -d - b\cos(2\pi x + \phi),\\ \frac{\partial \Psi}{\partial y} &= -1 \text{ at } y = h_1 \text{ and } y = h_2,\end{aligned} \tag{15}$$

$$\begin{aligned}\theta &= 0 \text{ on } y = h_1,\\ \theta &= 1 \text{ on } y = h_2,\end{aligned} \tag{16}$$

$$\begin{aligned}\Phi &= 0 \text{ on } y = h_1,\\ \Phi &= 1 \text{ on } y = h_2.\end{aligned} \tag{17}$$

where q is the flux in the wave frame, a, b, ϕ and d satisfy the relation

$$a^2 + b^2 + 2ab\cos\phi \le (1+d)^2.$$

Under the assumption of long wave length $\delta \ll 1$ and low Reynolds number, *Eqs.*(10) to (14) become

$$0 = -\frac{\partial p}{\partial x} + \frac{\partial}{\partial y}\left(\frac{1}{1+\lambda_1}\frac{\partial^2 \Psi}{\partial y^2}\right) + Gr\theta + B_r\Phi, \tag{18}$$

$$0 = -\frac{\partial p}{\partial y}, \tag{19}$$

$$\frac{1}{\Pr}\frac{\partial^2 \theta}{\partial y^2} + N_b \frac{\partial \theta}{\partial y}\frac{\partial \Phi}{\partial y} + N_T \left(\frac{\partial \theta}{\partial y}\right)^2 = 0. \tag{20}$$

$$\frac{\partial^2 \Phi}{\partial y^2} + \frac{N_T}{N_b}\frac{\partial^2 \theta}{\partial y^2} = 0 \tag{21}$$

Elimination of pressure from Eqs .(10) and (11), yields

$$\frac{\partial^2}{\partial y^2}\left[\frac{1}{1+\lambda_1}\frac{\partial^2 \Psi}{\partial y 2}\right] + Gr\frac{\partial \theta}{\partial y} + B_r \frac{\partial \Phi}{\partial y} = 0, \tag{22}$$

Solution of the problem

Homotopy perturbation method

Since Eq. (20) and (21) are coupled nonlinear equation so the exact solution of Eq. (20) and (21) are not possible. The Homotopy perturbation technique is applied to calculate the solution of the coupled nonlinear equations. For our convenience we have taken $L = \frac{\partial^2}{\partial y^2}$ as the linear operator. We define the initial guess as

$$\theta_{10} = \frac{h_1 - y}{h_1 - h_2},\ \Phi_{10} = \frac{h_1 - y}{h_1 - h_2}, \tag{23}$$

Using the similar procedure of Homotopy perturbation method as done in $[26-28]$, the solution of the Eq. (12) and (13) is straight forward written as

$$\begin{aligned}\theta = {} & \frac{h_1 - y}{h_1 - h_2} + \frac{\Pr N_T}{2(h_1 - h_2)^2}(1+N_b)(h_1^2 - y^2) + \frac{\Pr N_T}{2(h_1 - h_2)^3}(1+N_b)(h_1^2 - h_2^2)(y - h_1) \\ & + \frac{(\Pr N_T)^2 N_b}{6(h_1 - h_2)^3}(1+N_b)(h_1^3 - y^3) + \frac{(\Pr N_T)^2 N_b}{4(h_1 - h_2)^3}(1+N_b)(h_1 + h_2)(y^2 - h_1^2) \\ & + \frac{(\Pr N_T)^2 N_b}{4(h_1 - h_2)^3}(1+N_b)(h_1 + h_2)^2(h_1 - y) + \frac{(\Pr N_T)^2 N_b}{6(h_1 - h_2)^4}(1+N_b)(h_2^3 - h_1^3)(h_1 - y),\end{aligned} \tag{24}$$

$$\Phi = \frac{h_1 - y}{h_1 - h_2} + \frac{\Pr(N_T)^2(1+N_b)}{2N_b(h_1 - h_2)^2}\left((y^2 - h_1^2) + (h_1 + h_2)(h_1 - y)\right), \tag{25}$$

Using Eq. (24) and (25) the solution of Equation of Eq. (22) is defined as

$$\Psi = \frac{1}{360(h_1-h_2)^3}(-180h_2^3q + 3a_{02}h_1^7(h_2-y)^2 + 360h_2^3y - 3h_2(360h_2 + 5a_0h_2^4 + 2a_{01}h_2^5 + a_{02}h_2^6 - 360q)y^2 + (720h_2 + 30a_0h_2^4 + 9a_{01}h_2^5 + 4a_{02}h_2^6 - 720q)y^3 - 15a_0h_2^3y^4 - 3a_{01}h_2^3y^5 - a_{02}h_2^3y^6 + h_1^6(h_2-y)^2(6a_{01} - 5a_{02}h_2 - 4a_{02}y) + 15h_1^4(h_2-y)^2(-3a_0h_2 - 2a_0y + a_{01}h_2y) + 3h_1^5(h_2-y)^2(5a_0 - 4a_{01}h_2 - 3a_{01}y + 2a_{02}h_2y) - 3h_1^2(2a_{01}h_2^6 + a_{02}h_2^7 - 180h_2q + h_2(360 + 5a_{01}h_2^4 + 2a_{02}h_2^5)y - 2(180 + 5a_{01}h_2^4 + 2a_{02}h_2^5)y^2 + 3a_{01}h_2y^5 + a_{02}h_2y^6 + 5a_0h_2(h_2-y)^2(h_2^2 + 6h_2y + 3y^2)) + 3h_1(2a_{02}h_2^7y - 720h_2qy + 120(3q-2y)y^2 - 5h_2^4y^2(a_0 + a_{01}y) + h_2^6y(4a_{01} - a_{02}y) - 20h_2^3(6 + a_0y^3) + h_2^2(180q + 360y + 15a_0y^4 + 3a_{01}y^5 + a_{02}y^6) - 2h_2^5y(-5a_0 + y(a_{01} + a_{02}y))) + h_1^3(5a_{02}h_2^6 - 120a_0h_2^2y^2 - 180(q + 2y) + 15h_2^4(3a_{02} - a_{01}y) + 6h_2^5(2a_{01} - a_{02}y) + 60h_2(6 + a_0y^3) + y^4(15a_0 + y(3a_{01} + a_{02}y)))), \quad (26)$$

where the constants appearing in Eq. (26) is defined as

$$a_0 = \frac{(G_r + B_r)(1+\lambda_1)}{h_1 - h_2} - \frac{\Pr N_T}{2(h_1-h_2)^3}G_r(1+\lambda_1)(1+N_b)(h_1^2 - h_2^2) + \frac{B_r(1+\lambda_1)}{2N_b(h_1-h_2)^2}\Pr(N_T)^2(1+N_b)(h_1+h_2) + G_r(1+\lambda_1)(\Pr N_T)^2N_b(1+N_b)\left(\frac{(h_1+h_2)^2}{4(h_1-h_2)^3} + \frac{(h_2^3 - h_1^3)}{6(h_1-h_2)^4}\right),$$

$$a_{01} = \frac{G_r \Pr N_T(1+\lambda_1)(1+N_b)}{(h_1-h_2)^2} - \frac{G_r(1+\lambda_1)(\Pr N_T)^2N_b(1+N_b)(h_1+h_2)}{2(h_1-h_2)^3} - \frac{B_r(1+\lambda_1)\Pr(N_T)^2(1+N_b)}{N_b(h_1-h_2)^2}, \quad (27)$$

$$a_{02} = \frac{G_r(1+\lambda_1)(\Pr N_T)^2(1+N_b)}{2(h_1-h_2)^3}.$$

The axial pressure gradient is calculated from Eq. (18) by using Eq. (24) to (26) and is defined as

$$\frac{dp}{dx}=\frac{1}{60(h_1-h_2)^3 N_b(1+\lambda_1)}((3h_1^2h_2(6B_r(-5N_b+N_T^2(1+N_b)\Pr)$$
$$+G_rN_b(-30+N_T(1+N_b)\Pr(-6+N_T(-2+N_b)\Pr)))(1+\lambda_1)$$
$$-2h_1^3(3B_r(-5N_b+N_T^2(1+N_b)\Pr)+G_rN_b(-15-N_T(1+N_b)$$
$$\Pr(3+N_T(-2+N_b)\Pr)))(1+\lambda_1)+3h_1(-6B_rh_2^2N_T^2\Pr(1+\lambda_1)$$
$$+G_rh_2^2N_T^2N_b^3(\Pr)^2(1+\lambda_1)-G_rh_2^2N_TN_b^2\Pr(-6+N_T\Pr)(1+\lambda_1)$$
$$+N_b(-240-2h_2^2(3B_r(-5+N_T^2\Pr)+G_r(-15+N_T\Pr(-3+N_T\Pr)))(1+\lambda_1))$$
$$+2(360h_2N_b+h_2^3(3B_r(-5N_b+N_T^2(1+N_b)\Pr)+G_rN_b(-15+N_T$$
$$(1+N_b)\Pr(-3+N_T(-2+N_b)\Pr)))(1+\lambda_1)-5N_b(72q+$$
$$G_rN_T^2(-2+N_b)(1+N_b)(\Pr)^2y^3(1+\lambda_1))))), \quad 28$$

Expression for wave shape

The non- dimensional expressions for five considered wave form are given as

1) Sinusoidal wave

$$h_1(x)=1+a\sin 2\pi x,\quad h_2(x)=-d-b\sin(2\pi x+\phi).$$

2) Multisinusoidal wave

$$h_1(x)=1+a\sin 2n\pi x,\quad h_2(x)=-d-b\sin(2n\pi x+\phi).$$

3) Triangular wave

$$h_1(x)=1+a\left[\frac{8}{\pi^3}\sum_{m=1}^{\infty}\frac{(-1)^{m+1}}{(2m-1)^2}\sin(2\pi(2m-1)x)\right],$$

$$h_2(x)=-d-b\left[\frac{8}{\pi^3}\sum_{m=1}^{\infty}\frac{(-1)^{m+1}}{(2m-1)^2}\sin(2\pi(2m-1)x+\phi)\right].$$

4) Trapezoidal wave

$$h_1(x)=1+a\left[\frac{32}{\pi^2}\sum_{m=1}^{\infty}\frac{\sin\frac{\pi}{8}(2m-1)}{(2m-1)^2}\sin(2\pi(2m-1)x)\right],$$

$$h_2(x)=-d-b\left[\frac{32}{\pi^2}\sum_{m=1}^{\infty}\frac{\sin\frac{\pi}{8}(2m-1)}{(2m-1)^2}\sin(2\pi(2m-1)x+\phi)\right].$$

5) Square wave

$$h_1(x)=1+a\left[\frac{4}{\pi}\sum_{m=1}^{\infty}\frac{(-1)^{m+1}}{(2m-1)}\cos(2(2m-1)\pi x)\right],$$

$$h_2(x) = -d - b\left[\frac{4}{\pi}\sum_{m=1}^{\infty}\frac{(-1)^{m+1}}{(2m-1)}\cos\left(2(2m-1)\pi x + \phi\right)\right],$$

Numerical Results and Discussion

In this section the graphical results of the present problem is discussed. The expression for pressure rise and pressure gradient is calculated numerically using a mathematics software. Figs. 1 to 5 show the variation of pressure rise with volume flow rate Q for different values of width of the channel d, ratio of relaxation to retardation time λ_1, N_T thermophoresis parameter, amplitude ratio ϕ and G_r. It is observed from Figs. 1 and 2 that the pressure rise decreases in the retrograde pumping $(\Delta p > 0, Q < 0)$ and peristaltic pumping $(\Delta p > 0, Q > 0)$ regions with an increase in d and λ_1, while in copumping $(\Delta p < 0, Q > 0)$ region the pressure rise increases with an increase in d and λ_1. It is depicted from Fig. 3 that the behavior of the pressure rise is same in all the regions. Here the pressure rise decreases in all the regions with an increase in N_T. It is observed from Fig. 4 that with an increase in ϕ the pressure rise decreases in the retrograde pumping $(\Delta p > 0, Q < 0)$ and peristaltic pumping $(\Delta p > 0, Q > 0)$ regions, while in the copumping $(\Delta p < 0, Q > 0)$ region the behavior is quite opposite. It is observed from Fig. 5 that the pressure rise increases in all the regions with an increase in G_r. Figs. 6 to 11 show the variation of pressure gradient with the space coordinate x for different values of d, ϕ, N_T and Q. It is depicted from Figs. 6 to 8 that for $x \in [0, 0.2]$ and $x \in [0.8, 1]$, the pressure gradient is small i.e., the flow can easily pass without imposition of a large pressure gradient, while in the region $x \in [0.2, 0.8]$, the pressure gradient decreases with an increase in d, ϕ and N_T. So large pressure gradient is required to maintain the same flux. Figs. 9 to 11 show the variation of pressure gradient for different wave forms for different values of volume flow rate Q. Velocity profile for different values of Br, λ_1 and Q are shown in Figs. 12 to 14. It is depicted from Figs. 12 and 13 that $y \in [-1, 0]$ the magnitude value of the velocity profile decreases while in the region $y \in [1, 1.5]$ the magnitude value of the velocity profile increases. It is observed from Fig. 14 that the magnitude value of the velocity profile decreases with an increase in volume flow rate Q. Figs. 15 to 17 show the variation of temperature profile for different values of N_T, N_b and Pr. It is observed from Figs. 15 to 17 that the temperature profile increases with an increase in N_T, N_b and Pr. Concentration profile for different values of N_T, N_b and Pr are shown in Figs. 18 to 20. It is observed from Fig. 18 that the concentration profile decreases with an increase in N_T. It is depicted from Fig. 19 that the concentration profile increases with an increase in N_b. It is observed from Fig. 20 that the concentration profile decreases with an increase in Pr. Stream lines for different values of Gr, λ_1 and N_T are shown in Figs. 21, 22 and 23. It is observed from Fig. 21 that with an increase in Gr the size of the trapped bolus increases in the upper half of the channel and decreases in the lower half of the channel. Moreover the bolus in the symmetric channel is in the middle of the channel (see panels (a) and (c)) while in the asymmetric the bolus shifted towards the left side of the channel due to

phase angle (see panels (b) and (d)). It is depicted from Fig. 22 that the size of the trapped bolus increases with an increase in λ_1. Moreover the size of the trapped bolus is small in asymmetric channel as compared with the symmetric channel. It is observed from Fig. 23 that the size of the trapped bolus decreases in the upper and lower half of the channel. Fig. 24 shows the stream lines for different wave form.

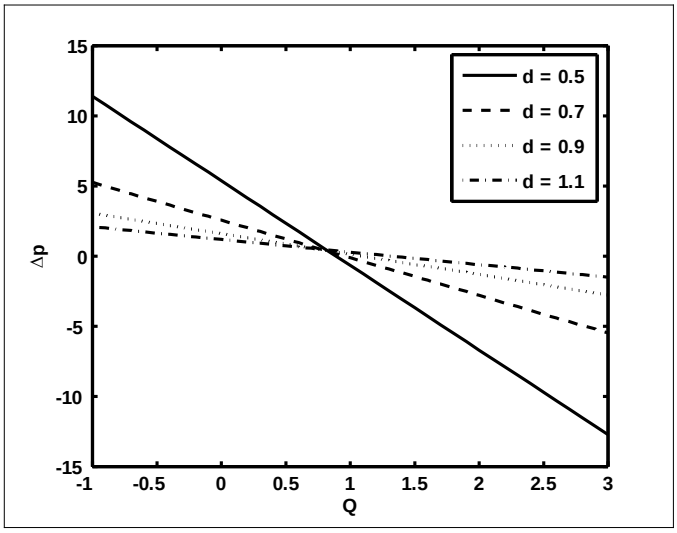

Fig.1

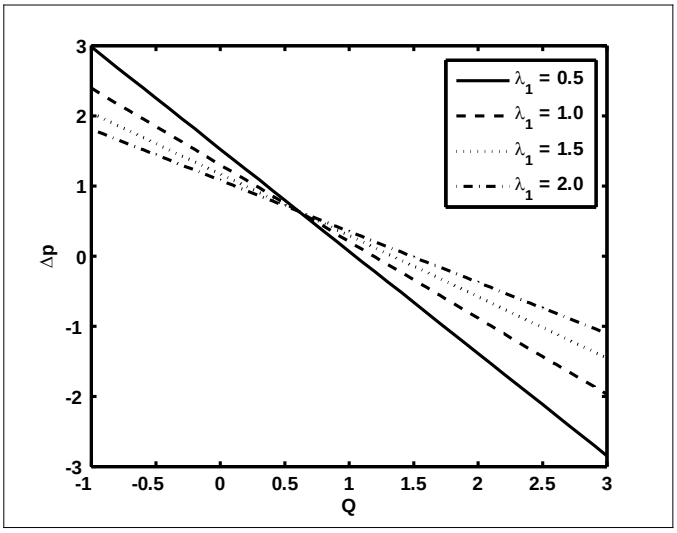

Fig. 2

Fig. 1 : Variation of pressure rise Δp with volume flow rate Q for different values of d for fixed $a=0.7,\ b=0.7,\ \phi=\frac{\pi}{2},\ N_b=0.5,\ \Pr=2,\ N_T=0.9,\ Br=0.9,\ G_r=0.8,$ $\lambda_1=2.$

Fig .2 : Variation of pressure rise Δp with volume flow rate Q for different values of λ_1 for fixed $a=0.7,\ b=0.7,\ \mathrm{N}_b=0.5,\ \Pr=2,\ N_T=0.9,\ \phi=\frac{\pi}{2},\ Br=0.9,\ G_r=0.8,$ $d=1.22.$

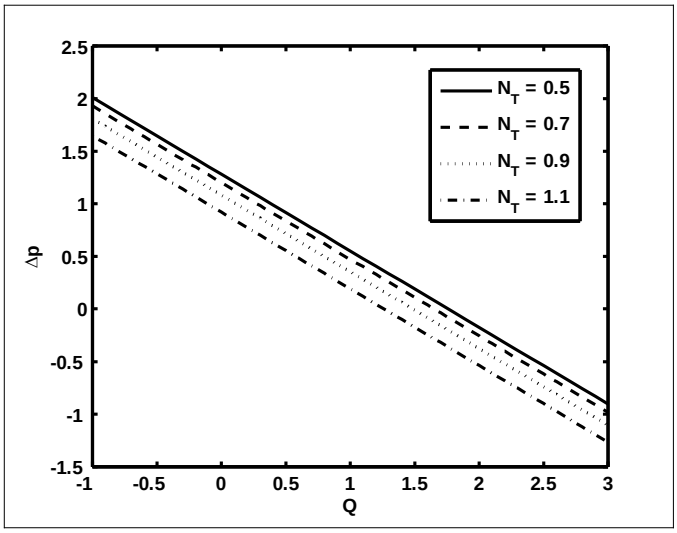

Fig. 3

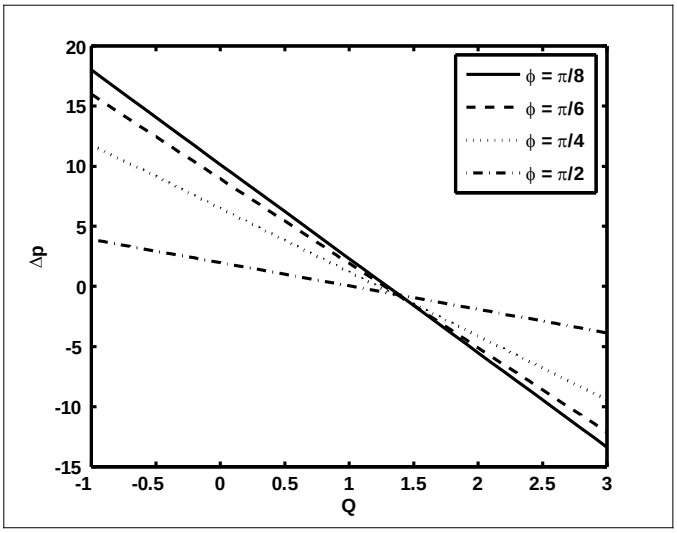

Fig. 4

Fig .3 : Variation of pressure rise Δp with volume flow rate Q for different values of N_T for fixed $a = 0.7,\quad b = 0.7,\quad \phi = \frac{\pi}{2},\quad N_b = 0.5,\quad \Pr = 2,\quad d = 1.2,\quad Br = 0.9,\quad G_r = 0.8,$ $\lambda_1 = 2.$

Fig .4 : Variation of pressure rise Δp with volume flow rate Q for different values of ϕ for fixed $a = 0.7,\quad b = 0.7,\quad d = 0.8,\quad N_b = 0.5,\quad \Pr = 2,\quad N_T = 0.9,\quad Br = 0.9,\quad G_r = 0.8,$ $\lambda_1 = 2.$

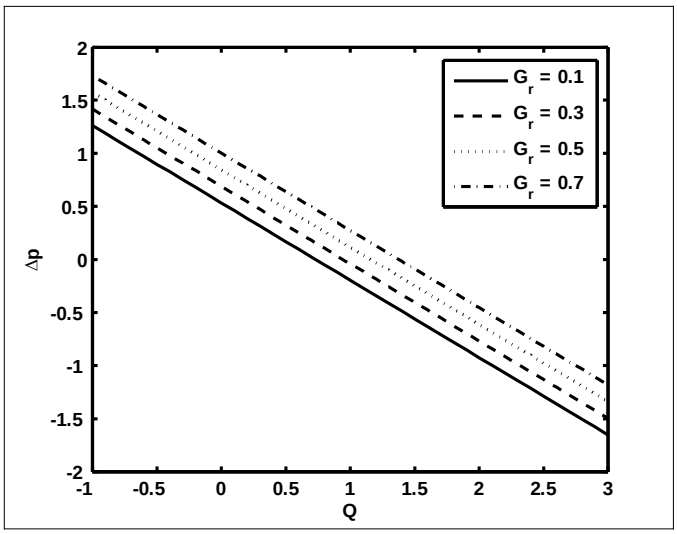

Fig. 5

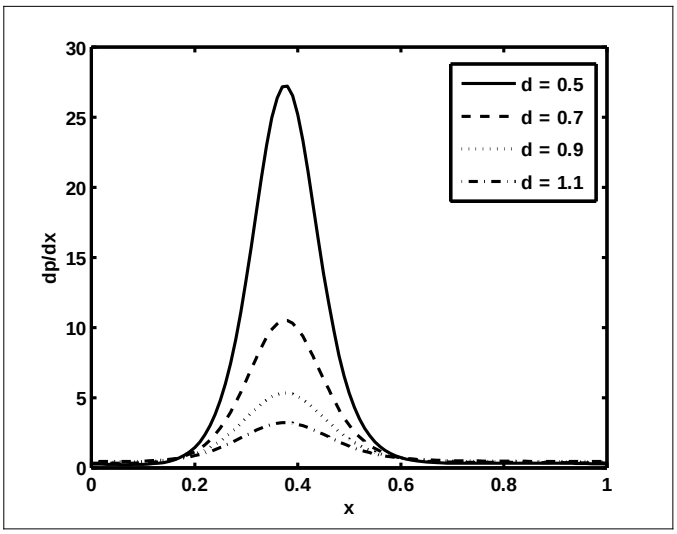

Fig. 6

Fig .5 : Variation of pressure rise Δp with volume flow rate Q for different values of G_r for fixed $a = 0.7,\ b = 0.7,\ \phi = \frac{\pi}{2},\ N_b = 0.5,\ \Pr = 2,\ d = 1.2,\ Br = 0.9,\ N_T = 0.9,\ \lambda_1 = 2.$

Fig .6 : Variation of pressure gradient dp/dx with x for different values of d for fixed $a = 0.7,\ b = 0.7\ ,\ \phi = \frac{\pi}{2},\ N_b = 0.5,\ \Pr = 2,\ N_T = 0.9,\ Br = 0.9,\ G_r = 0.8,\ \lambda_1 = 2,\ Q = 0.1.$

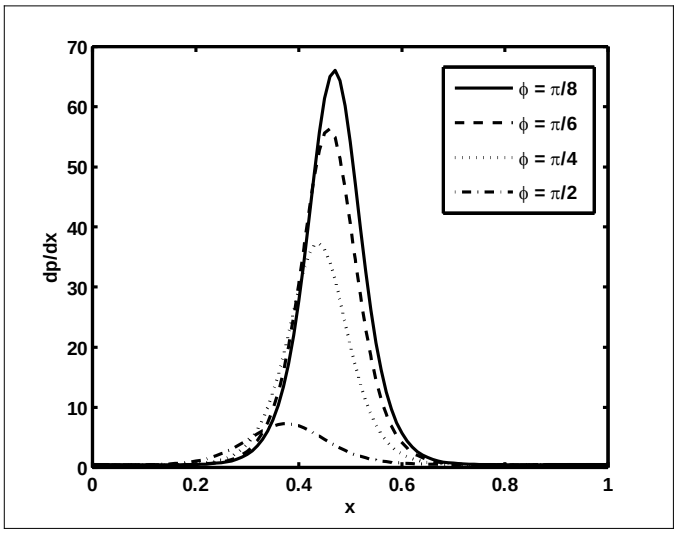

Fig. 7

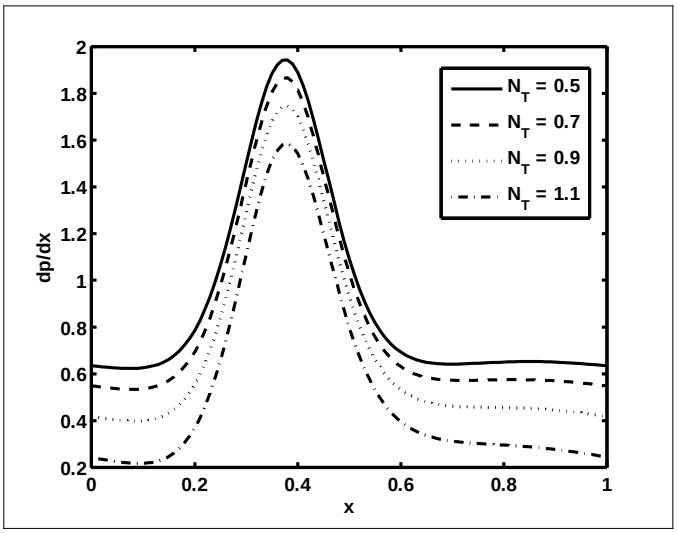

Fig. 8

Fig .7 : Variation of pressure gradient dp/dx with x for different values of λ for fixed $a = 0.7,\ b = 0.7\ ,\ d = 0.8,\ N_b = 0.5,\ \Pr = 2,\ N_T = 0.9,\ Br = 0.9,\ G_r = 0.8,\ \lambda_1 = 2,\ Q = 0.1.$

Fig .8 : Variation of pressure gradient dp/dx with x for different values of N_T for fixed $a = 0.7,\ b = 0.7\ ,\ d = 1.2,\ N_b = 0.5,\ \Pr = 2,\ \phi = \frac{\pi}{2},\ Br = 0.9,\ G_r = 0.8,\ \lambda_1 = 2,\ Q = 0.5.$

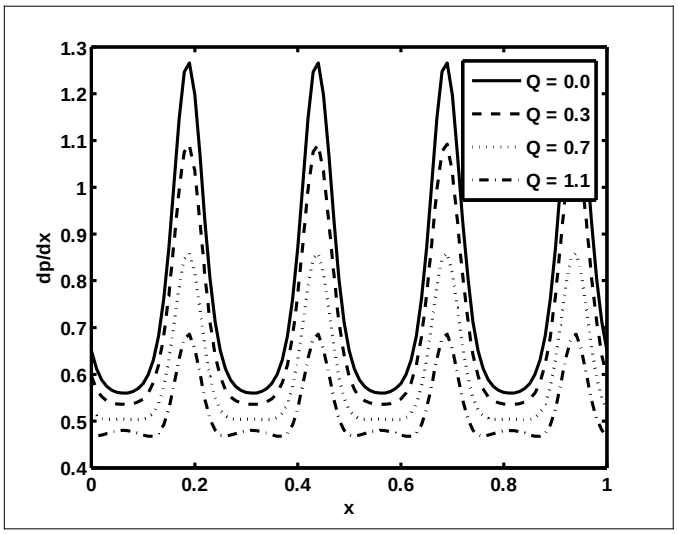

Fig. 9

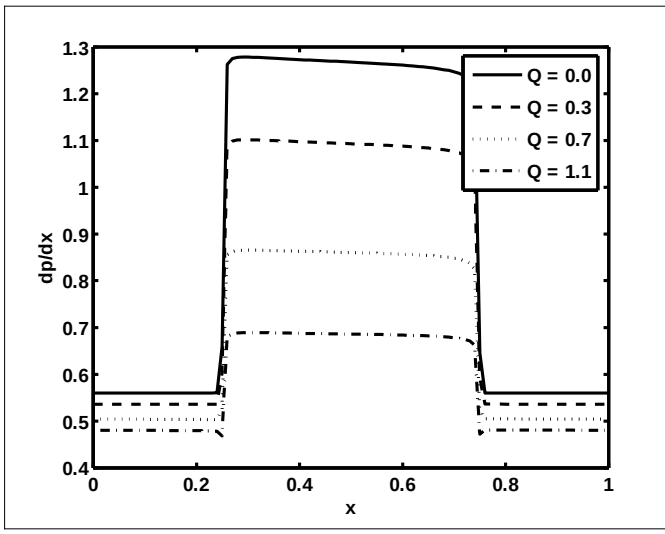

Fig. 10

Fig .9 : Variation of pressure gradient dp/dx with x for different values of Q for multisinusoidal wave. The other parameters are $a = 0.8,\quad b = 0.1\ ,\ d = 1.8,\quad N_b = 0.5,$ $\Pr = 2,\quad \phi = 0.1,\quad Br = 0.9,\quad G_r = 0.8,\quad \lambda_1 = 2,\quad N_T = 0.9,\quad n = 4.$

Fig .10 : Variation of pressure gradient dp/dx with x for different values of Q for square wave. The other parameters are $a = 0.8,\quad b = 0.1\ ,\ d = 1.8,\quad N_b = 0.5,\quad \Pr = 2,\quad \phi = 0.1,$ $Br = 0.9,\quad G_r = 0.8,\quad \lambda_1 = 2,\quad N_T = 0.9.$

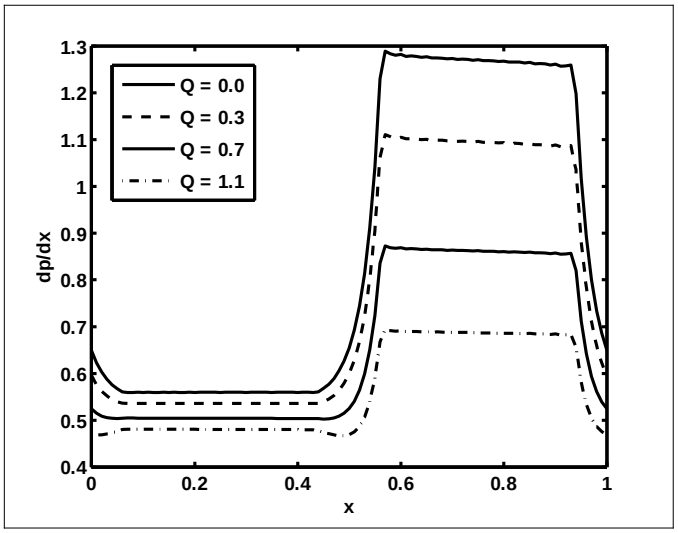

Fig. 11

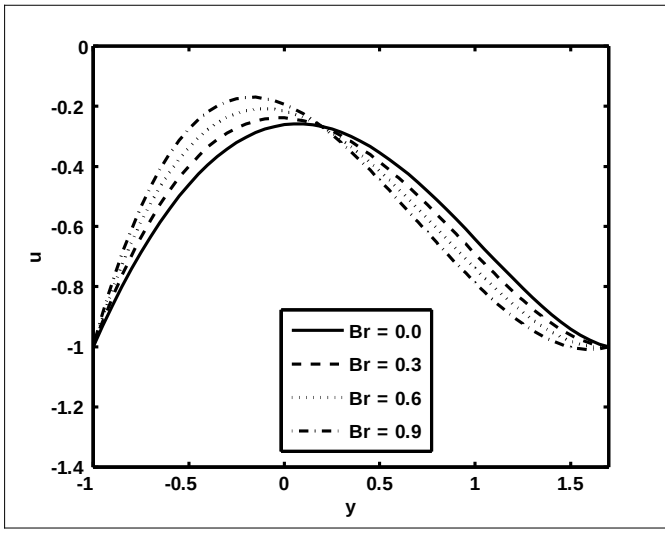

Fig. 12

Fig .11 : Variation of pressure gradient dp/dx with x for different values of Q for trapezoidal wave. The other parameters are $a=0.8,\quad b=0.1\ ,\ d=1.8,\quad N_b=0.5,\quad \Pr=2,$ $\phi=0.1,\quad Br=0.9,\quad G_r=0.8,\quad \lambda_1=2,\quad N_T=0.9.$

Fig .12 : Velocity profile for different values of Br for fixed values of $a=0.7,\quad b=0.7,$ $d=1,\quad \phi=\frac{\pi}{2},\quad N_T=0.9,\quad N_b=0.5,\quad \Pr=2,\quad Q=0.5,\quad Gr=0.8,\quad x=0,\quad \lambda_1=2.$

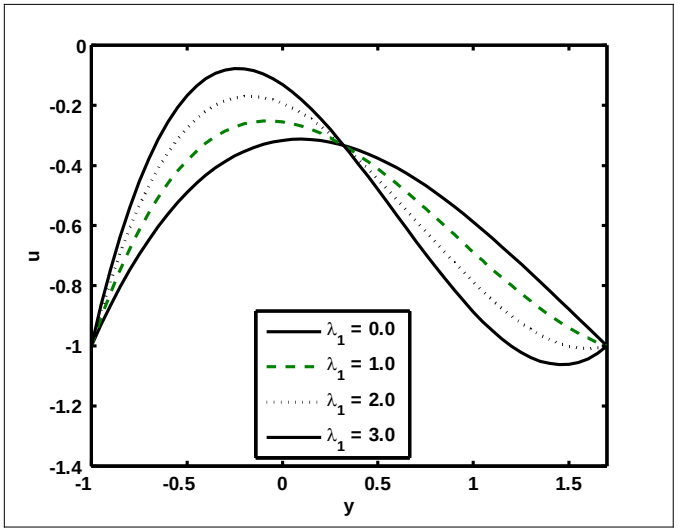

Fig. 13

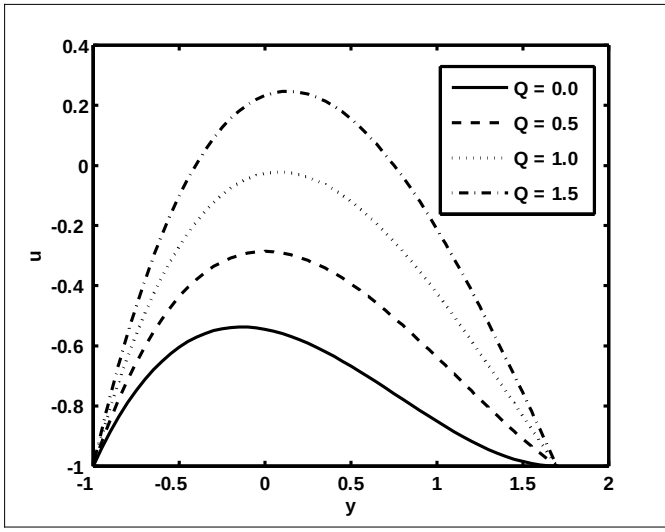

Fig. 14

Fig .13 : Velocity profile for different values of λ_1 for fixed values of $a=0.7,\quad b=0.7,$ $d=1,\quad \phi=\frac{\pi}{2},\quad N_T=0.9,\quad N_b=0.5,\quad \Pr=2,\quad Q=0.5,\quad Gr=0.8,\quad x=0,\quad B_r=0.9.$

Fig .14 : Velocity profile for different values of Q for fixed values of $a=0.7,\quad b=0.7,$ $d=1,\quad \phi=\frac{\pi}{2},\quad N_T=0.9,\quad N_b=0.5,\quad \Pr=2,\quad \lambda_1=0.5,\quad Gr=0.8,\quad x=0,\quad B_r=0.9.$

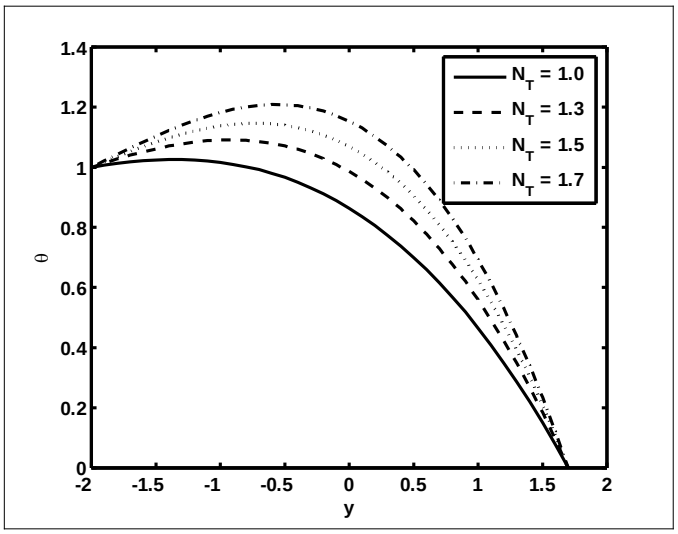

Fig. 15

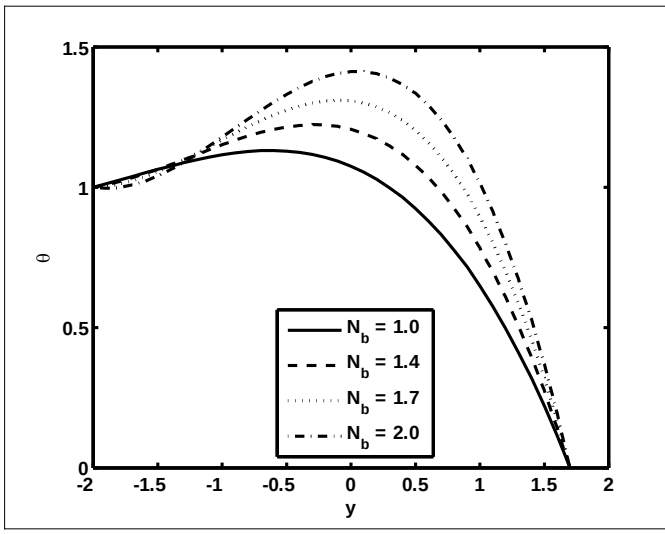

Fig. 16

Fig .15 : Temperature profile for different values of N_T for fixed values of $a = 0.7,\quad b = 1.2,$ $d = 2,\quad N_b = 0.6,\quad x = 0,\quad \Pr = 2,\quad \phi = \frac{\pi}{2}.$

Fig .16 : Temperature profile for different values of N_b for fixed values of $a = 0.7,\quad b = 1.2,$ $d = 2,\quad N_T = 1.2,\quad x = 0,\quad \Pr = 2,\quad \phi = \frac{\pi}{2}.$

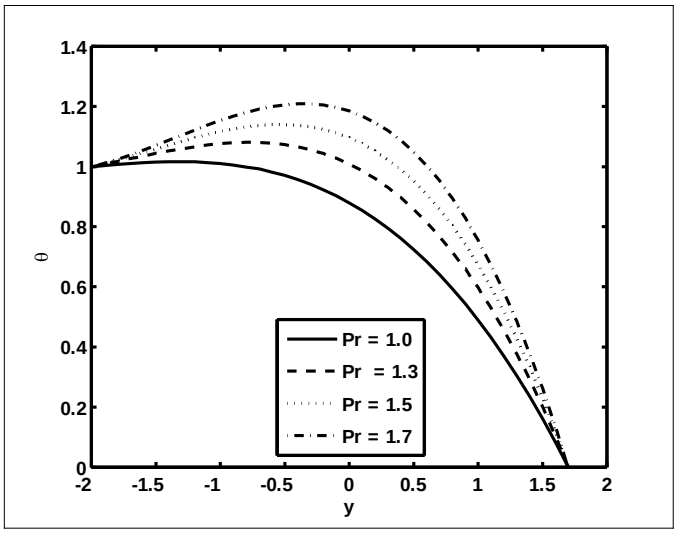

Fig. 17

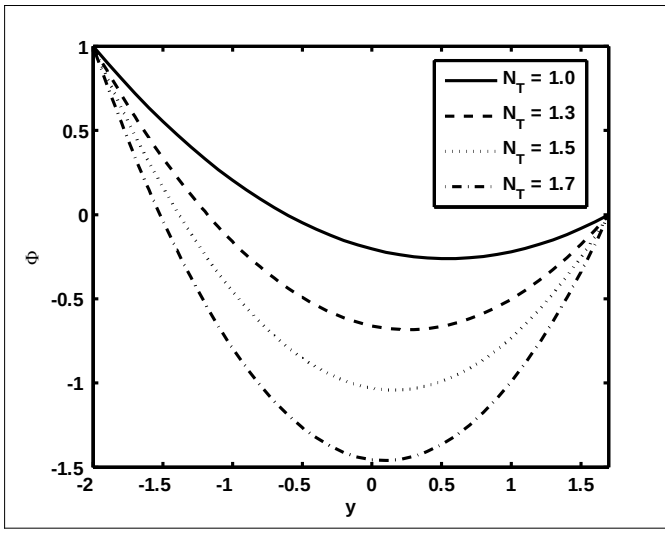

Fig. 18

Fig .17 : Temperature profile for different values of Pr for fixed values of $a = 0.7,\quad b = 1.2,$ $d = 2,\quad N_T = 1.5,\quad x = 0,\quad N_b = 1.2,\quad \phi = \frac{\pi}{2}.$

Fig .18 : Concentration profile for different values of N_T for fixed values of $a = 0.7$, $b = 1.2$, $d = 2$, $N_b = 0.6$, $x = 0$, $\Pr = 2$, $\phi = \frac{\pi}{2}$.

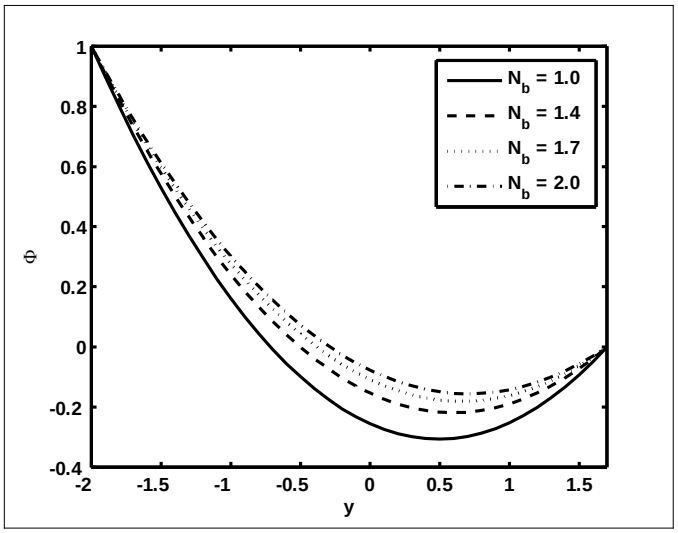

Fig. 19

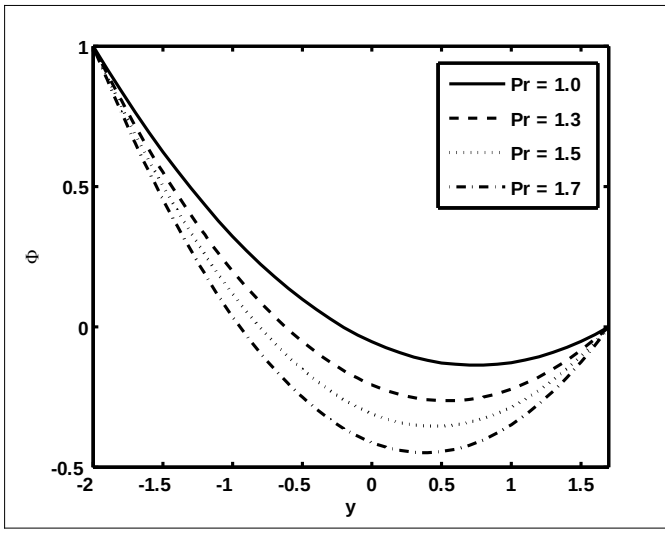

Fig. 20

Fig .19 : Concentration profile for different values of N_b for fixed values of $a = 0.7$, $b = 1.2$, $d = 2$, $N_T = 1.2$, $x = 0$, $\Pr = 2$, $\phi = \frac{\pi}{2}$.

Fig .20 : Concentration profile for different values of $\Pr$ for fixed values of $a = 0.7$, $b = 1.2$, $d = 2$, $N_T = 1.5$, $x = 0$, $N_b = 1.2$, $\phi = \frac{\pi}{2}$.

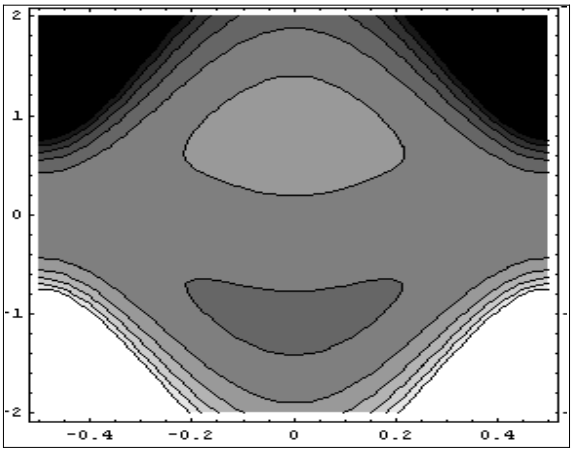

Fig. (a) for $\phi = 0$ and $Gr = 0.1$.

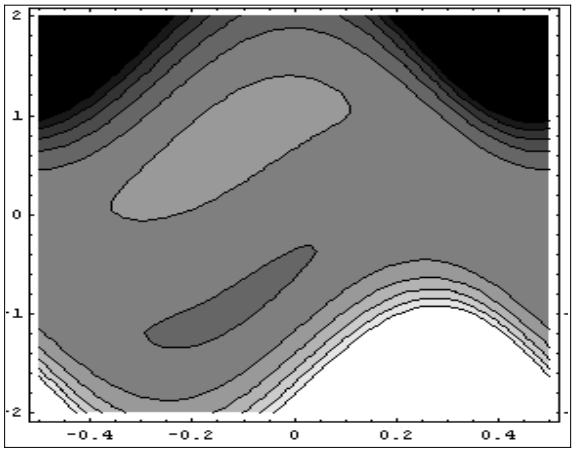

Fig. (b) for $\phi = \frac{\pi}{2}$ and $Gr = 0.1$.

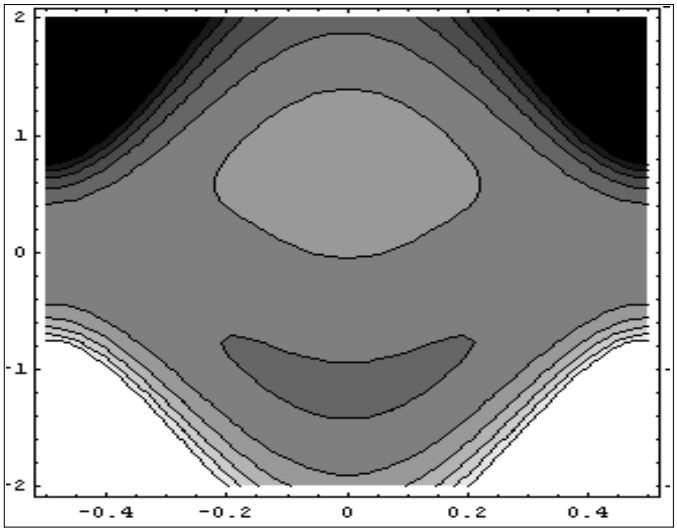

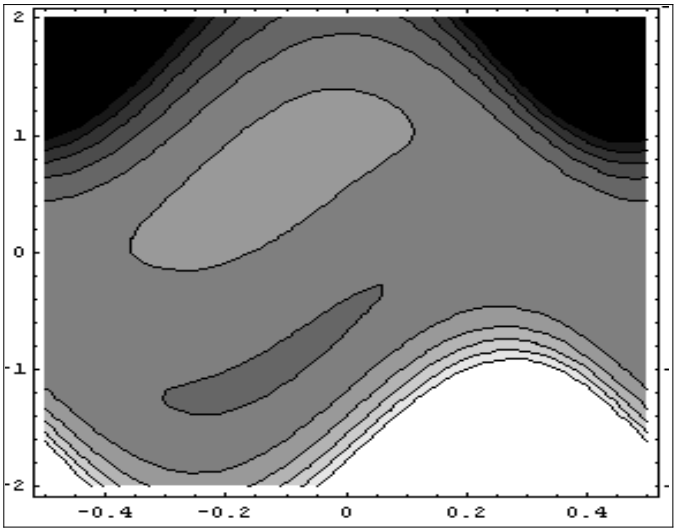

Fig (c) for $\phi = 0$ and $Gr = 0.9$. Fig. (d) for $\phi = \frac{\pi}{2}$ and $Gr = 0.9$.

Fig .21 : Stream lines for different values of Gr. The other parameters are $a = 0.7,\quad b = 0.7,$ $d = 1,\quad N_T = 0.9,\quad N_b = 0.5,\quad \Pr = 1,\quad \lambda_1 = 0.5,\quad B_r = 0.9,\quad Q = 2.$

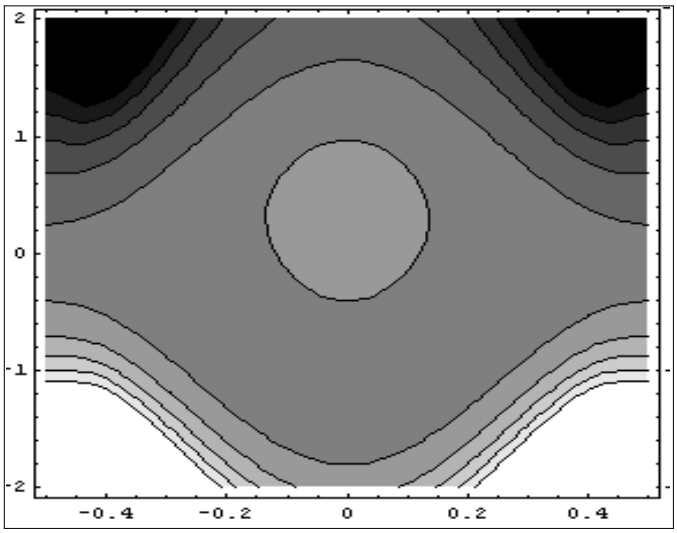

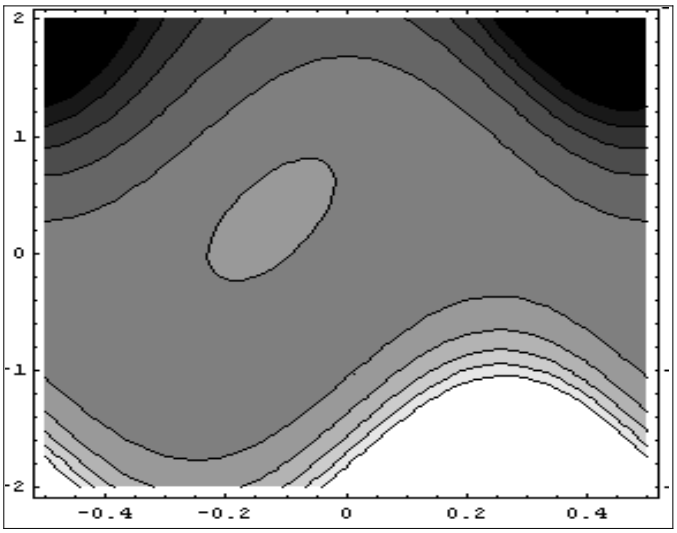

Fig. (a) for $\phi = 0$ and $\lambda_1 = 2.$ Fig. (b) for $\phi = \frac{\pi}{2}$ and $\lambda_1 = 2.$

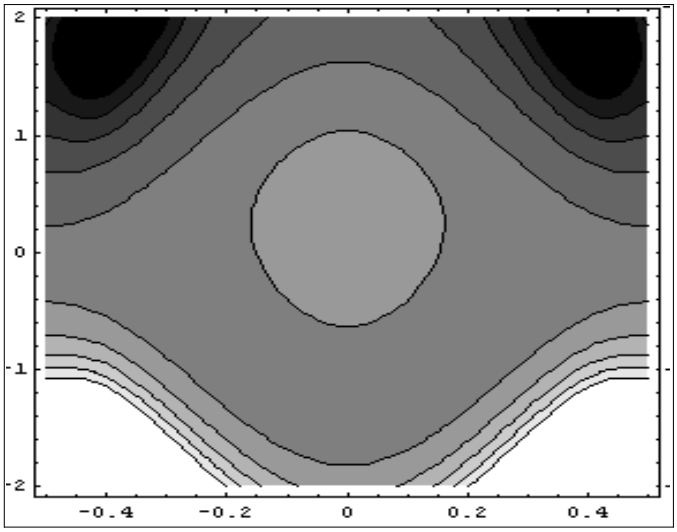

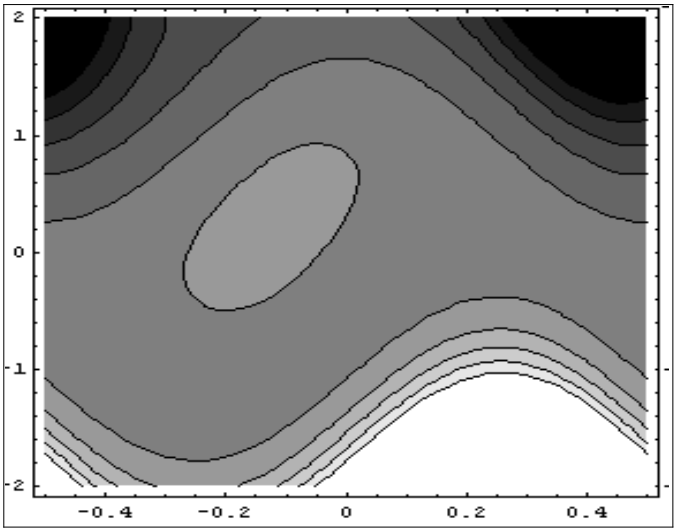

Fig. (c) for $\phi = 0$ and $\lambda_1 = 3.$ Fig. (d) for $\phi = \frac{\pi}{2}$ and $\lambda_1 = 3.$

Fig. 22 : Stream lines for different values of λ_1. The other parameters are $a = 0.7,\quad b = 0.7,$ $d = 1,\quad N_T = 0.9,\quad N_b = 0.5,\quad \Pr = 1,\quad \lambda_1 = 2,\quad Gr = 0.8,\quad B_r = 0.9,\quad Q = 1.5.$

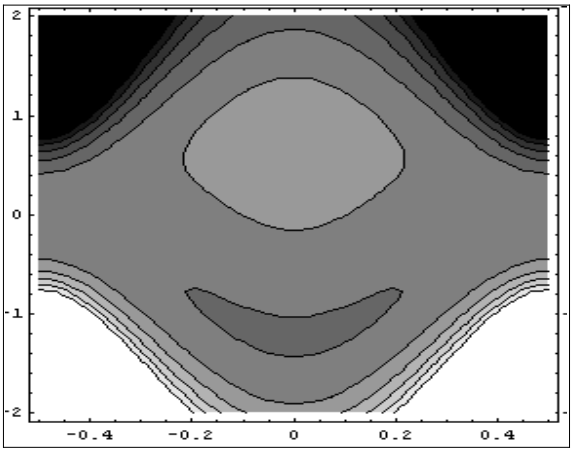

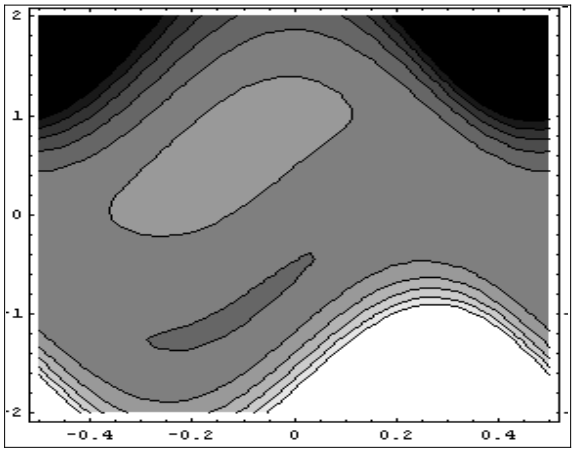

Fig. (a) for $\phi = 0$ and $N_T = 1.0.$ Fig. (b) $\phi = \frac{\pi}{2}$ and $N_T = 1.6.$

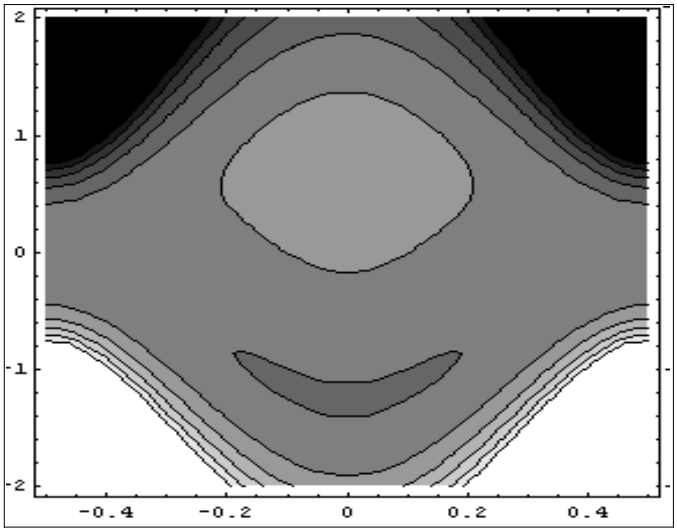

Fig. (c) for $\phi = 0$ and $N_T = 1.0$.

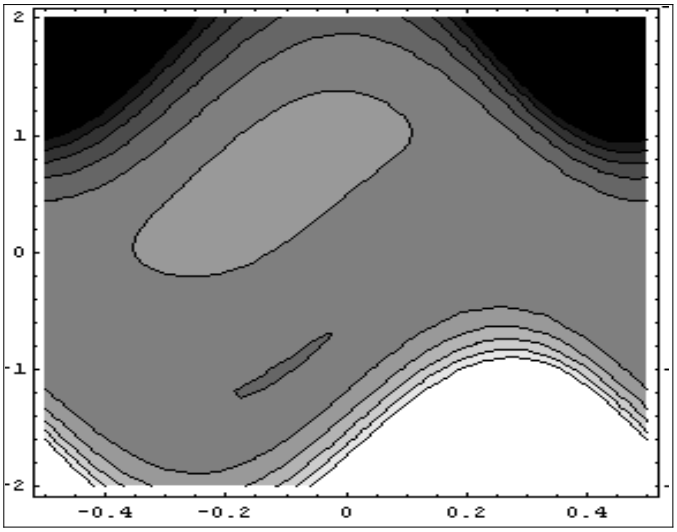

Fig. (d) for $\phi = \frac{\pi}{2}$ and $N_T = 1.6$.

Fig .23 : Stream lines for different values of N_T. The other parameters are $a = 0.7$, $b = 0.7$, $d = 1$, $\lambda_1 = 1$, $N_b = 0.5$, $\Pr = 1$, $Gr = 0.8$, $B_r = 0.9$, $Q = 2$.

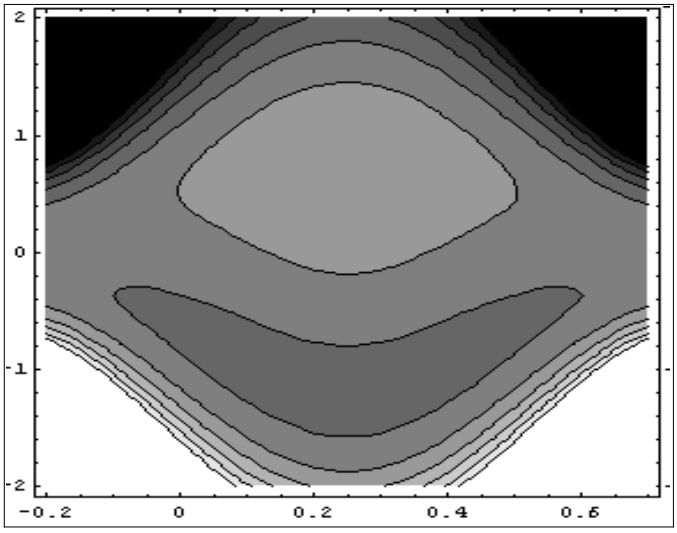

Fig. (a) for sinusoidal wave

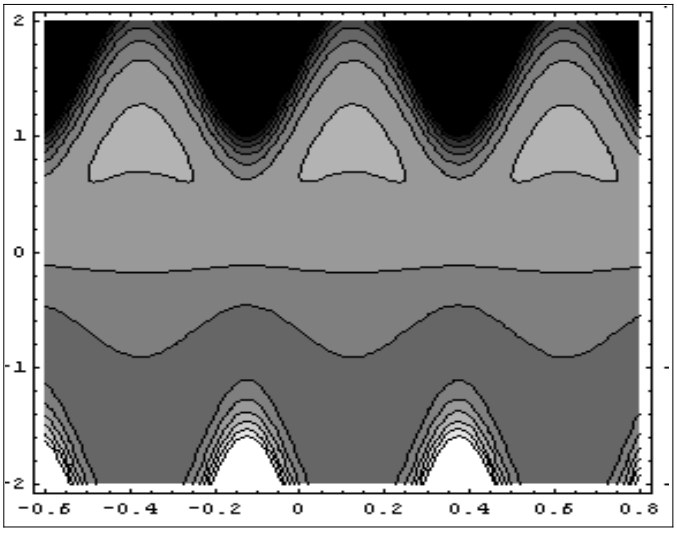

Fig. (b) for multisinusoidal wave

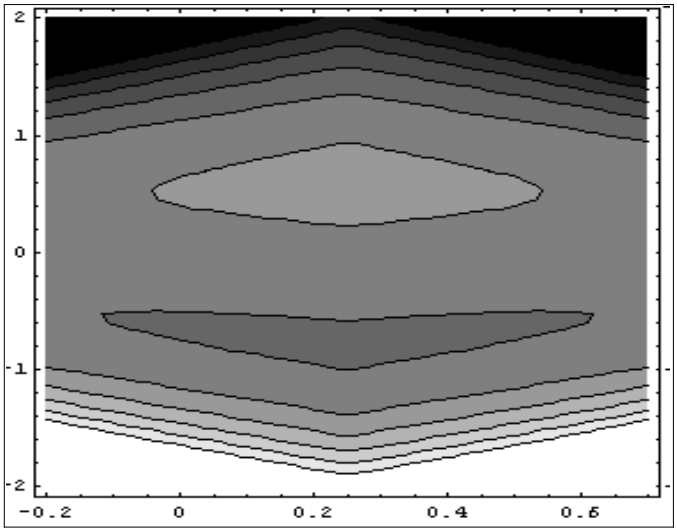

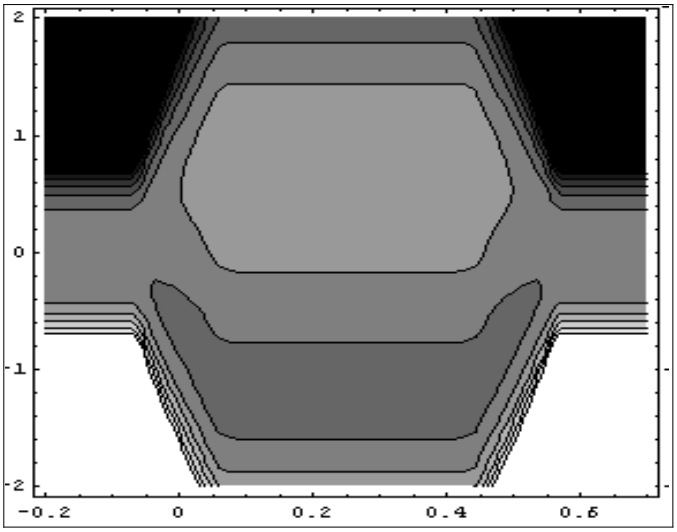

Fig. (*c*) for Triangular wave Fig. (*d*) for Trapezoidal wave

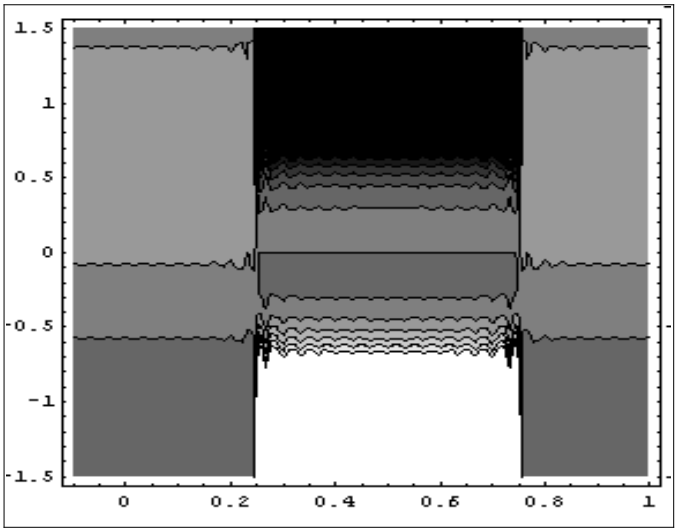

Fig. (*e*) for Square wave

Fig. 24 : Stream lines for different wave forms for fixed values of $a = 0.7,\quad b = 0.7,\quad d = 1,$ $\phi = 0.0,\quad N_T = 0.9,\quad N_b = 0.5,\quad \Pr = 1,\quad \lambda_1 = 2,\quad Gr = 0.1,\quad B_r = 0.9,\quad Q = 2.$

Conclusion

This paper presents the peristaltic flow of a nanofluid in an asymmetric channel. The governing two dimensional equations have been modeled and then simplified using long wave length

approximation. The governing equations of temperature and nano particle volume fraction are coupled and solved analytically using a Homotopy perturbation method. The exact solutions have been calculated for the stream functions, velocity profile and pressure gradient. The results are discussed through graphs. The main finding can be summarized as follows:

1. It is observed that the pressure rise decreases in the retrograde pumping and peristaltic pumping regions with an increase in d , ϕ and λ_1, while in copumping region the pressure rise increases with an increase in d , ϕ and λ_1.

2. The pressure gradient decreases with an increase in d , ϕ and N_T.

3. The temperature profile increases with an increase in $N_{T,}$ N_b and $\Pr$.

4. The concentration profile decreases with an increase in N_T and $\Pr$ while the concentration profile increases with an increase in N_b.

5. The size of the trapped bolus increases in the upper half of the channel and decreases in the lower half of the channel with an increase in Gr.

6. The size of the trapped bolus increases with an increase in λ_1 .

Acknowledgement

This work was supported by the grant under WCU (World Class University) program through the National Research Foundation of Korea (NRF) funded by the Ministry of Education, Science and Technology R31-2008-000-10049-0.

References

1. K.K. Raju, R. Devanathan, Peristaltic motion of a non-Newtonian fluid, Rheologica Acta, 11(1972)170 – 178.
2. K.K. Raju, R. Devanathan, Peristaltic motion of a non-Newtonian fluid-II, Rheologica Acta, 13 (1974), p. 944 .
3. M. Nakamura and T. Sawada, Numerical study on the flow of a non-Newtonian fluid through an axisymmetric stenosis, Journal of Biomechanical Engineering, 110(1988)137 – 143.
4. J. C. T. Eijkle, A. van der Berg, Nanofluidics: what is it and what can we expect from it?, Microfluid Nanofluid 1(2005)249 – 267.
5. G. B ohme and R. Friedrich, Peristaltic flow of viscoelastic liquids, Journal of Fluid Mechanics, 128(1983)109 – 122.
6. T. Hayat, Y. Wang, K. Hutter, S. Asghar, and A. M. Siddiqui, Peristaltic transport of an oldroyd-b fluid in a planar channel, Mathematical Problems in Engineering, 2004(2004)347 – 376.
7. R. S. Agarwal and C. Dhanapal, Numerical solution to the flow of amicropolar fluid between porous walls of different permeability, International Journal of Engineering

Science, 25(1987)325 – 336.

8. K. S. Mekheimer and M. A. El-kot, The micropolar fluid model for blood flow through astenotic arteries, International Journal of Pure and Applied Mathematical, 36(2007)393.
9. S. Nadeem, Safia Akram, Peristaltic flow of a Williamson fluid in an asymmetric channel, Communications in Nonlinear Science and Numerical Simulation 15(2010)1705 – 1716.
10. S. Nadeem, Safia Akram, Slip effects on the peristaltic flow of a Jeffrey fluid in an asymmetric channel under the effect of induced magnetic field, International Journal for Numerical Methods in fluids 63(2010)374 – 394.
11. S. Nadeem, Noreen Sher Akbar, Influence of heat transfer on a peristaltic transport of a Herschel-Bulkley fluid in a non-uniform tube, Communications in Nonlinear Science and Numerical Simulation 14(2009)4100 – 4113.
12. S. Nadeem, Safia Akram, Influence of inclined magnetic field on peristaltic flow of a Jeffrey fluid with heat and mass transfer in an inclined symmetric or asymmetric channel, Asia-Pacific Journal of Chemical Engineering, DOI: 10.1002/apj.488.
13. S. Srinivas, M. Kothandapani, The influence of heat and mass transfer om MHD peristaltic flow through a porous space with complaints walls, Applied Mathematics and Computation 213(2009)197 – 208.
14. E. F. Elshehawey, M. E. Elsayed Elbarbary, S. Nasser Elgazery, Effects of inclined magnetic field on magneto fluid flow through a porous medium between two inclined wavy porous plates (numerical study), Applied Mathematics and Computation 135(2003)85 – 103.
15. S. Nadeem, Safia Akram, Peristaltic flow of a Jeffrey fluid in a rectangular duct, Nonlinear Analysis: Real World Applications 11(2010)42384247.
16. D. Srinivasacharya, M. Mishra, and A. R. Rao, Peristaltic pumping of a micropolar fluid in a tube, Acta Mechanica 161(2003)165 – 178.
17. R. Girija Devi and R. Devanathan, Peristaltic transport of micropolar fluid, Indian National Science Academy 81(1995)149 – 163.
18. J. C. T. Eijkle, and A. van der Berg, Nanofluidics: what is it and what can we expect from it?, Microfluid Nanofluid 1(2005)249 – 267.
19. S. U. S Choi, Enhancing thermal conductivity of fluid with nanoparticles.developments and Applications of non-Newtonian Flow, ASME FED 66(231)99 – 105.
20. O. D. Makinde, A. Aziz, Boundary layer flow of a nanofluid past a stretching sheet with a convective boundary condition, International Journal of Thermal Sciences 50(2011)1326 – 1332.
21. N. Bachok, A. Ishak, I. Pop, Boundary-layer flow of nanofluids over a moving surface in a flowing fluid, International Journal of Thermal Sciences 49(2010)1663 – 1668.
22. M. Akbari, A. Behzadmehr, F. Shahraki, Fully developed mixed convection in horizontal and inclined tubes with uniform heat flux using nanofluid, International Journal of Heat and Fluid Flow 29(2008)545 – 556.
23. A.V. Kuznetsov, D.A. Nield, Natural convective boundary-layer flow of a nanofluid past a vertical plate, International Journal of Thermal Sciences 49(2010)243 – 247.

24. K.B. Anoop, T. Sundararajan, Sarit K. Das, Effect of particle size on the convective heat transfer in nanofluid in the developing region, International Journal of Heat and Mass Transfer 52(2009)2189 – 2195.
25. Y.Z. Yang, G. Zhang, E.A. Grulke, W.B. Anderson, G. Wu, Heat transfer properties of nanoparticle-in-fluid dispersions (nanofluids) in laminar flow, International Journal of Heat and Mass Transfer 48(2005)1107 – 1116.
26. D. D. Ganji, A. Sadighi, Application of He's Homotopy-perturbation Method to Nonlinear Coupled Systems of Reaction-diffusion Equations, International Journal of Nonlinear Sciences and Numerical Simulation, 7(2006)411 – 418.
27. D.D. Ganji, The application of He's homotopy perturbation method to non-linear equations arising in heat transfer, Physics Letters A, 355(2006)337 – 341.
28. D. D. Ganji, A. Rajabi, Assessment of homotopy--perturbation and perturbation methods in heat radiation equations, International Communications in Heat and Mass Transfer, 33(2006)391 – 400.